Earthquake Geotechnical Engineering for Protection and Development of Environment and Constructions – Silvestri & Moraci (Eds)
© 2019 Associazione Geotecnica Italiana, Rome, Italy, ISBN 978-0-367-14328-2

Kinematic and inertial seismic load effects on pile foundations in stratified soil

T.K. Garala & S.P.G. Madabhushi
Schofield Centre, Department of Engineering, University of Cambridge, UK

ABSTRACT: A series of centrifuge experiments were performed with pile foundations in stratified soil to investigate the kinematic and inertial load effects during earthquakes. A single aluminium model pile was embedded into a soft kaolin clay overlying the dense sand. Each experiment was carried out in two flights, to study the kinematic and inertial load effects separately. A few important findings of this study are: (i) the kinematic load induced pile bending is equally important as inertial load induced pile bending during the smaller intensity base excitations, (ii) the bending moment due to inertial loads is predominant in comparison to kinematic bending moment during the larger intensity base excitations, and (iii) the existing methods in literature for determining the pile kinematic bending moment at the interface of two-layered soils are underestimating the bending moment. However, the recently proposed methods are resulting in a better estimation than the old conventional methods.

1 PROBLEM DEFINITION

Pile foundations are extensively used on land and offshore to transfer superstructure loads to deeper layers of soil, relying on skin-friction and end-bearing. During the earthquakes, the deformation of surrounding soil induces the kinematic loads and vibrations of superstructure cause inertial loads onto the pile foundations. It is difficult to identify the predominant load on the pile foundations during earthquakes, especially in stratified soil, as kinematic and inertial loads act together. In this study, an attempt is made to understand the kinematic and inertial loads acting on a single pile embedded in a stratified soil using the high gravity dynamic centrifuge testing.

2 CENTRIFUGE MODELLING

Field stress-strain conditions can be obtained in a scaled-down model of a geotechnical structure by subjecting the model to increased g-field using a centrifuge. In this research, the Turner beam centrifuge (Schofield 1980) at Schofield Centre, University of Cambridge, was used to test the scaled centrifuge models at 60 times the earth's gravity. Servo-hydraulic earthquake shaker was used to fire the required model earthquakes. Equivalent shear beam (ESB) box was used as a container to prepare the model.

2.1 *Materials and model construction*

2.1.1 *Materials*

A layered soil profile with considerable stiffness contrast between the soil layers can lead to the significant kinematic effects on the pile foundations. Therefore, a soil profile with dense poorly graded fraction-B Leighton Buzzard (LB) sand underlying the soft speswhite kaolin clay was prepared. Tables 1 and 2 show the properties of fraction-B LB sand and speswhite kaolin clay respectively.

Table 1. Properties of fraction-B Leighton Buzzard (LB) sand.

Property	Value
Specific gravity, G_s	2.65
Maximum void ratio, e_{max}	0.767
Minimum void ratio, e_{min}	0.49
Effective particle size, D_{10} (mm)	0.68
Average particle size, D_{50} (mm)	0.80
Coefficient of uniformity, C_u	1.221
Coefficient of curvature, C_c	0.97

Table 2. Properties of speswhite kaolin clay (Lau 2015).

Property	Value
Plastic limit, PL (%)	30
Liquid limit, LL (%)	63
Specific gravity, G_s	2.60
Slope of critical state line (CSL) in q′-p plane	0.90
Slope of an unload-reload line, (κ)	0.039
Intercept of CSL at p'=1 kPa (Γ)	3.31
Slope of normal consolidation line (λ)	0.22

2.1.2 *Model pile foundation*

A strain gauged aluminium tubular model pile of length (l) 300mm, outer diameter (d_o) 11.1mm and thickness (t) 0.9mm was used to replicate a prototype pile in this study. The flexural stiffness of the prototype pile is equivalent to a 0.7m diameter high strength concrete pile. Perspex having negligible mass was used as the pile cap in flight-01 (F1) and a brass cap was used in flight-02 (F2). The brass cap will induce a static vertical force of 167.75N at model scale (603.9kN at prototype scale) in F2. This vertical force is half the axial load carrying capacity of the single pile.

2.1.3 *Model preparation and centrifuge testing*

The sand layer of thickness 130mm was prepared at 1g by pouring the sand into the ESB box using the automatic sand pouring machine. The relative density of the sand was obtained as around 82±2%. The sand layer was saturated using deaired water with 5-10mm of extra water at the top of the sand layer to minimise any air entry during the clay pouring. Clay slurry was prepared by mixing the speswhite kaolin clay powder and de-aired water in 1:1.25 ratio under the vacuum. The prepared clay slurry was filled into the ESB box to the required depth. The ESB box with clay slurry and the sand layer was placed on a computer-controlled hydraulic press to consolidate under the required vertical stress.

The depth of the clay layer after consolidation and trimming for the levelled surface was 150mm with a saturated unit weight of 16.41 kN/m^3. Piezo-electric accelerometers (PAs) and micro-electro-mechanical systems accelerometers (MEMSs) were used to measure the accelerations in the soil profile and pile foundation respectively. Figure 1 shows the cross-section of the model in which the location of the instruments can also be seen with prototype dimensions being mentioned within the parentheses. Pile foundation was installed manually at 1g at an approximate rate of 2-4 mm/s in clay. A manual hydraulic jack was used to embed the pile into the sand up to a depth of 80mm (~7.20d_o) at an approximate rate 0.5-1 mm/s.

The experiment was carried out at 60g and in two flights. In F1, the experiment was carried out with negligible mass perspex as a pile cap to get the effects of kinematic load alone. While in F2, the mass was added at pile cap level to represent the forces induced by a superstructure. Therefore, the pile foundation was subjected to both kinematic and inertial loads in F2. Six different base excitations (BEs) were chosen for this study and the model was subjected to

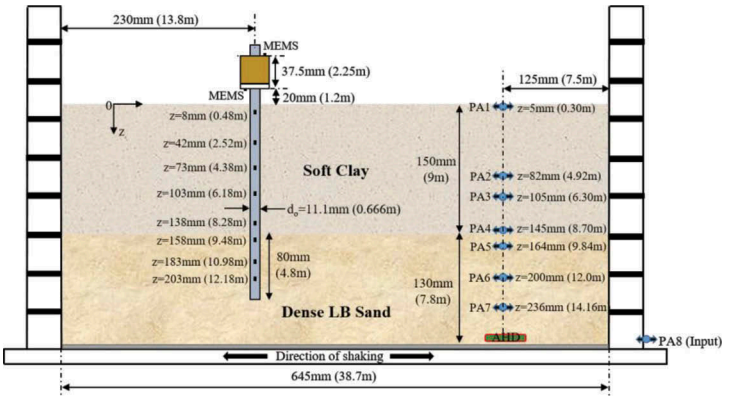

Figure 1. Cross-sectional view of the model.

Table 3. Base excitations considered in this study (at prototype scale).

Base excitation	*Signal*	*Frequency (Hz)*	*Peak acceleration (g)*
BE1	Sinusoidal	0.667	0.044
BE3	Sine-sweep	0.3 to 2.5	0.052
BE4	Sinusoidal	0.667	0.176

these six BEs in both the flights. However, the results obtained from only a few BEs will be discussed in this article and the characteristics of these BEs are shown in Table 3. BE3 was used to determine the natural frequency of the soil profile and pile foundation. BE1 and BE4 were used to compare the pile accelerations and pile bending moments for two different shaking intensities at the same frequency. The following section discusses the preliminary results of these centrifuge experiments. The results are presented at the prototype scale, except where stated as model scale.

3 RESULTS AND DISCUSSION

3.1 *Strength and stiffness of the soil layers*

A T-bar test (Lau 2015) was performed on the clay layer in the centrifuge at 60g to determine the undrained shear strength (c_u) of the clay before firing the earthquakes in F1. Figure 2a shows the measured c_u profile along the depth. The small strain shear modulus (G_0) of the soil layers were determined using the air hammer device before and after firing the model earthquakes in both the flights of the experiment and shown in Figure 2b.

Figure 2b depicts that the stiffness of the clay layer slightly decreased after the six BEs in F1. This may be due to the clay softening happened due to the six BEs. Due to the possible drainage from both the top and bottom of the clay layer, the stiffness got increased before F2 and dropped again after the six BEs in F2. No significant change in the sand layer stiffness was observed before and after the earthquakes in both the flights.

3.2 *Natural frequency of the soil profile and pile foundation*

A sine-sweep excitation with the frequencies ranging between 0.3 to 2.5 Hz was fired as BE3 in both the flights to determine the natural frequency of the soil profile and pile foundation. Figures 3a and 3b show the acceleration-time history plots during the F1 and F2 respectively. Figure 3a conveys that the pile foundation follows the soil movement during the earthquakes

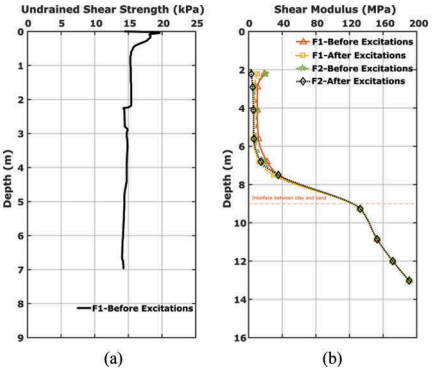

Figure 2. (a) Undrained shear strength of clay and (b) stiffness of tested soil layers.

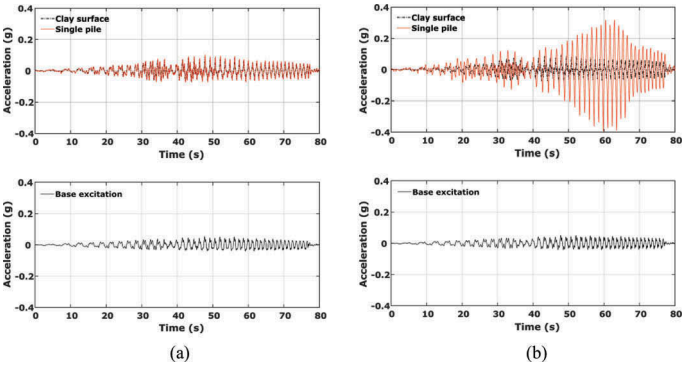

Figure 3. Acceleration recorded at the clay surface and single pile for BE3 (a) Flight-01 and (b) Flight-02.

in the absence of inertial load. However, as expected, the pile is responding differently from the soil movement when the pile is carrying some vertical load as seen in Figure 3b. Further, a significant acceleration amplification at a certain time instant can be observed for the single pile in Figure 3b. The fast Fourier transform (FFT) of base excitations, clay surface and pile foundation accelerations in both the flights are computed. The FFTs of clay surface and pile foundation are normalised with the FFT of base excitation and plotted in Figure 4 as the amplification ratio against the frequency. Two clear peaks can be seen at around 0.78 Hz and

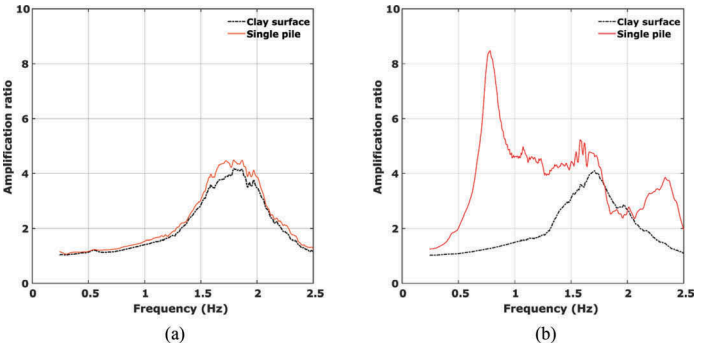

Figure 4. Amplification ratio of the clay surface and single pile for BE3 (a) Flight-01 and (b) Flight-02.

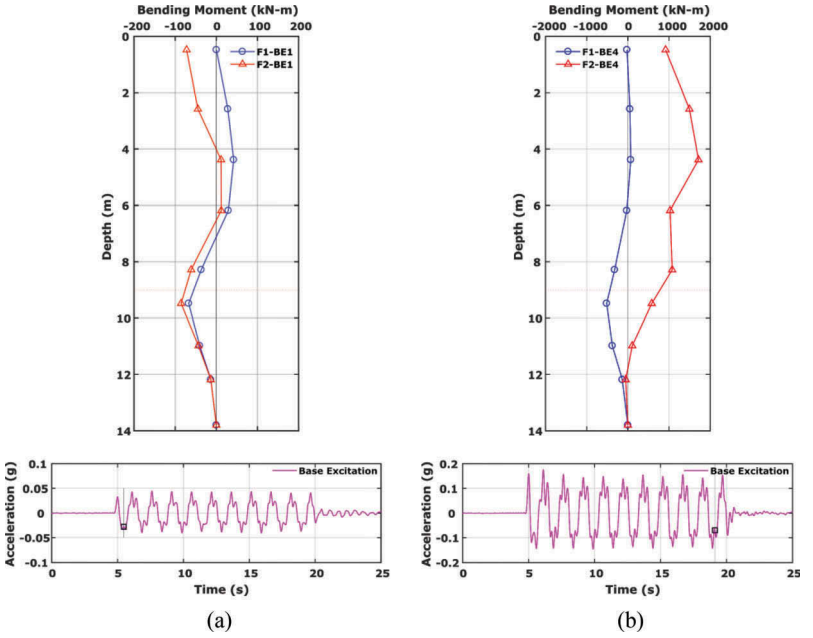

Figure 5. Bending moment at a certain instant of base excitation for (a) BE1 and (b) BE4.

1.7 Hz in Figure 4b, indicating the natural frequency (f) of the single pile foundation and soil profile tested respectively.

3.3 *Bending moments in the pile foundation*

The two-layered soil model with the pile foundation was subjected to a 0.667 Hz sinusoidal shake with two different intensities of 0.044g (BE1) and 0.176g (BE4). This enables to investigate the effect of kinematic and inertial loads on the pile foundation at smaller and larger intensities of the base excitation at a frequency close to the natural frequency of the pile foundation in F2. In this study, the bending moment at the tip of the pile foundation is assumed as zero in both the flights. Figure 5a shows the bending moment measured along the pile depth at a certain instant of time during both the flights for BE1. It conveys that the inertial loads are dominant only at the shallower depths (around $10d_o$) and the kinematic loads are predominant after that. Similarly, Figure 5b shows the bending moment measured during the BE4 in both the flights. In this case, the effect of the inertial load was extended to greater depths compared to BE1. Also, the difference between bending moments from F1 and F2 is significantly greater during BE4 in comparison to BE1.

Figure 6 shows the maximum bending moment measured at different locations along the pile. The maximum bending moment during the F1 (see Figure 6a) is occurring near the interface of the soil layers. This is expected considering the fact that sharp variation of shear modulus between the soil layers can impose significant pile curvature demands at the interface of soil layers. However, due to the inertial load in F2, the maximum bending moment is occurring at the upper portion of the pile, irrespective of the intensity of base excitation. In both the flights and during both the BEs, with an increase in the intensity of the BE, the peak bending moment value increases, but the effect is predominant during the presence of the inertial load. It should be noted that the peak bending moment during F1 (Figure 5) is shown slightly beneath the interface due to the non-availability of the data at the interface. Further, a simple linear fit is used to join all the data points. Using a continuous polynomial or spline fits between the data points can predict the peak bending moment at the interface and this value

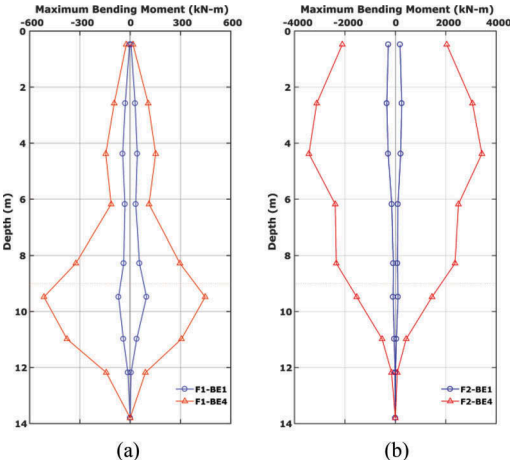

Figure 6. Maximum bending moment envelope during (a) Flight-01 and (b) Flight-02.

may be greater or lesser than the reported peak bending moment in this study. It is also worth mentioning that the frequency of BE1 and BE4 are close to the natural frequency of the pile foundation in F2 and hence the bending moments due to the inertial load effects are significantly higher than the kinematic load induced bending moments. The bending moments due to the kinematic load can be larger if the BE frequency is close to the natural frequency of the soil stratum. However, this aspect was not studied in this paper.

3.4 *Comparison of experimental maximum kinematic bending moment with literature methods*

Table 4 lists some of the methods available in the literature to compute the pile kinematic bending moment (M_k) at the interface of two-layered soils during the earthquakes. The methods that do not require any ground response analysis are only considered for the comparison with the centrifuge data obtained in this study. The earlier conventional design methods used to assume that the pile follows the surrounding soil motion and determines the M_k by computing the free-field soil curvature. However, these methods do not consider the soil geometry characteristics, pile dimensions and soil-pile interaction. Overcoming some of the drawbacks of these methods, Dobry & O'Rourke (1983) proposed an analytical solution considering the stiffness contrast between the soil layers and soil-pile interaction. Nevertheless, the thickness of soil layers and excitation frequency effects are not included in this method. Nikolaou & Gazetas (1997) proposed an equation for determining the harmonic steady state M_k under resonant conditions. This equation is based on a characteristic shear stress (τ_c), which is a function of maximum free-field surface acceleration (a_s). The M_k determined under transient seismic excitations using Nikolaou & Gazetas (1997) are smaller than the steady-state M_k by a factor of about 3 to 5 (Nikolaou et al. 2001). Later, Mylonakis (2001) proposed an equation for determining M_k considering the effect of thickness of the soil layers, dynamic nature of excitation and soil damping. The frequency effects are incorporated using an amplification factor (φ). In recent times, Di Laora et al. (2012) performed extensive 3D dynamic finite element analyses for various pile-soil configurations and proposed three equations for computing maximum M_k based on the availability of either maximum transient shear strain at the interface ($\gamma_{1,dyn}$), surface acceleration (a_s) or rock acceleration (a_r). Di Laora et al. (2012) considered a stress reduction factor of one while calculating the shear strain using surface acceleration. This will result in an upper bound value to the true shear strain at the depth under consideration.

The literature methods shown in Table 4 are developed assuming both soil and pile as linear elastic or equivalent linear viscoelastic materials and hence cannot be applicable for stronger intensity base excitations where the soil and pile behaviours can be non-linear. Therefore,

Table 4. Methods to compute the pile kinematic bending moment.

Study	Method	Equation
Dobry & O'Rourke (1983)	Analytical solution using the beam on Winkler foundation	$M_k = 1.86(E_p I_p)^{0.75}(G_1)^{0.25}\gamma_1 F$ $F = \frac{(1-c^{-4})(1+c^3)}{(1+c)(c^{-1}+1+c+c^2)};\ c = \left(\frac{G_2}{G_1}\right)^{0.25}$
Nikolaou & Gazetas (1997)	Regression analysis using the beam on dynamic Winkler foundation	$M_k = 0.042\ \tau_c d^3 \left(\frac{L}{d}\right)^{0.30}\left(\frac{E_p}{E_1}\right)^{0.65}\left(\frac{V_2}{V_1}\right)^{0.50}$ $\tau_c \approx a_s \rho_1 h_1$
Mylonakis (2001)	Analytical solution using the beam on dynamic Winkler foundation	$M_k = (E_p I_p)\left(\frac{\varepsilon_p}{\gamma_1}\right)_{\omega=0}\gamma_1\ \left(\frac{\varphi}{r}\right)$ $\left(\frac{\varepsilon_p}{\gamma_1}\right)_{\omega=0} = \frac{(c^2-c+1)\left\{\left[3\left(\frac{k_1}{E_p}\right)^{0.25}\left(\frac{h_1}{d}\right)-1\right]c(c-1)-1\right\}}{2c^4\left(\frac{h_1}{d}\right)}$ $\gamma_1 = \frac{r_d \rho_1 h_1 a_s}{G_1};\ r_d = r_d(z) \cong 1 - 0.015z$ $\varphi\ \cong 1 \sim 1.25;\ c = \left(\frac{G_2}{G_1}\right)^{0.25}$
Di Laora et al. (2012)	Regression analysis using three-dimensional finite element analyses	$M_k = \frac{2E_p I_p}{d}\left(\frac{\varepsilon_p}{\gamma_1}\right)_{\omega=0}\frac{\tau_c}{G_1}\varphi_s$ $\varepsilon_p = \chi\gamma_1\left[-0.5\left(\frac{h_1}{d}\right)^{-1} + \left(\frac{E_p}{E_1}\right)^{-0.25}(c-1)^{0.5}\right]$ $c = \left(\frac{G_2}{G_1}\right)^{0.25};\ \varphi_s \cong 1.00;\ \chi \cong 0.93$

E_p is the Young's modulus of the pile; G_1 and G_2 are the shear modulus values of top and bottom layers of layered soil respectively; I_p is the cross-sectional moment of inertia of pile; M_k is the pile bending moment due to kinematic loads from surrounding soil; V_1 and V_2 are the shear wave velocities of the top and bottom layers of layered soil respectively; r_d is the depth factor; a_s is the free-field acceleration at the surface; γ_1 is the shear strain in the top layer of the soil; ε_p is the pile bending strain; ρ_1 is the mass density of the top layer; τ_c is the characteristic shear stress; d is the pile diameter; h_1 is the thickness of the top layer; k_1 is the spring coefficient; L is the length of the pile in soil; r is the radius of the pile; z is the depth from the ground surface; φ and φ_s are the frequency factors or amplification factors; χ is the regression coefficient; ω is the angular frequency.

peak kinematic bending moment measured during the smaller intensity base excitation (BE1) was only compared with the literature methods. An average shear modulus of 18 MPa and 186 MPa (see Figure 2b) are considered for top soft clay and bottom dense sand layers respectively. The equivalent prototype pile dimensions, 0.666m diameter solid concrete pile with a flexural rigidity of 344 MNm^2, were used in the computations as most of the methods in the literature are applicable only for solid cylindrical piles. The peak surface acceleration (0.074g) recorded close to the clay surface (see Figure 7a) was used in computing the τ_c and peak shear strain (γ_1) in the clay layer. A $\varphi$of 1.25 was used for computing the M_k from Mylonakis (2001). Figure 7b shows the comparison and as it shows the literature methods are under estimating the M_k in comparison to the experimentally determined M_k. Among all the methods considered in this study, Di Laora et al. (2012) results in a better estimation of the M_k with the least percentage difference of around 19% with the experimentally determined M_k. On the other hand, Nikolaou & Gazetas (1997) ends up with the highest percentage difference of around 85% with the experimentally determined M_k. Moreover, the M_k obtained by Nikolaou & Gazetas (1997) is not reduced for transient seismic conditions. Therefore, the percentage difference further increases if the computed M_k from Nikolaou & Gazetas (1997) is reduced by a factor of 3 to 5 to consider the frequency effects as recommended by Nikolaou et al. (2001). For some of the literature methods, the consideration of soil stiffness degradation during this smaller intensity base excitation might give M_k close to the experimental values, however, this is beyond the scope of this paper.

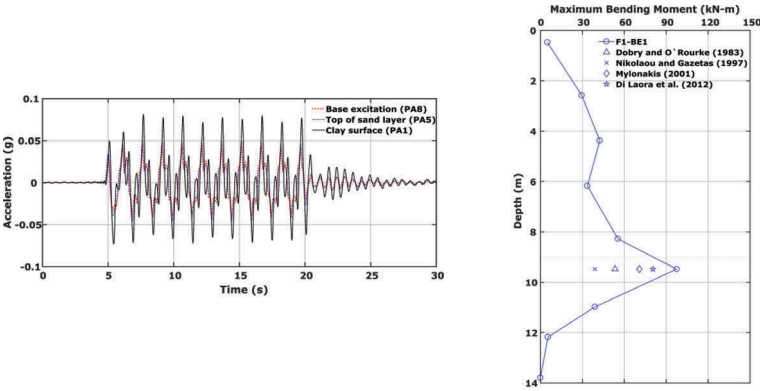

(a) (b)

Figure 7. (a) Free-field accelerations measured during BE1 of F1 and (b) comparison of maximum kinematic bending moment obtained from centrifuge test and literature methods for BE1 of F1.

4 CONCLUSIONS

A series of dynamic centrifuge experiments were carried out on pile foundations embedded in a two-layered soil profile. During the smaller intensity base excitation, it was observed that the pile foundation follows the soil movement in the absence of the inertial load on the pile. Further, the comparison of peak kinematic bending moments (M_k) from centrifuge experiments with the literature methods conveys that these methods are underestimating the M_k even for a smaller intensity base excitation. However, the M_k determined from the recently developed methods are giving a better estimation than the old conventional methods. Contrarily, as expected, the pile is responding differently from the ground movement in the presence of vertical loads at the top of the pile. Also, the pile bending due to kinematic loads is of comparable magnitude to the inertial load induced pile bending during the smaller intensity base excitation, though they occur at different locations in the pile foundation. Conversely, during the larger intensity excitation, the bending moment due to the inertial load is dominant than the kinematic load induced bending moment.

ACKNOWLEDGEMENTS

The first author would like to thank Dr Raffaele Di Laora, University of Campania Luigi Vanvitelli, Italy for his technical discussions. The authors also appreciate the anonymous reviewer's feedback on this article.

REFERENCES

Di Laora, R., Mandolini, A. & Mylonakis, G. 2012. Insight on Kinematic Bending of Flexible Piles in Layered Soil. *Soil Dynamics and Earthquake Engineering* 43: 309–322.

Dobry, R. & O'Rourke M.J. 1983. Discussion of 'Seismic response of end-bearing piles' by Flores Berrones, R. & Whitman, R.V. *Journal of Geotechnical Engineering* 109(5): 778–781.

Lau, B.H. 2015. *Cyclic behaviour of monopile foundations for offshore wind turbines in clay*. PhD Dissertation, University of Cambridge.

Mylonakis, G. 2001. Simplified method for seismic pile bending at soil-layer interfaces. *Soils and Foundations* 41(4): 47–58.

Nikolaou A.S. & Gazetas, G. 1997. Seismic design procedure for kinematically loaded piles. *Proc. 14th Int. Conf. Soil Mech. Found. Engineering, ISSMFE TC4 Earthquake geo. engg.*: 253–260. Hamburg.

Nikolaou, A.S., Mylonakis, G., Gazetas, G. & Tazoh, T. 2001. Kinematic pile bending during earthquakes: analysis and field measurements. *Geotechnique* 51(5): 425–440.

Schofield, A.N. 1980. Cambridge geotechnical centrifuge operations. *Geotechnique* 30(3): 227–268.